위핑 유동 조건에서의 직사각형 체 주위 유동의 수력학적 분석

호산나 우위톤즈[*] · 이인원[†]

Hydrodynamic Analysis of Rectangular Sieve Tray under Weeping Conditions

Hosanna Uwitonze[*] and Inwon Lee[†]

Abstract Within fractionating devices existing in separation and purification industries, sieve trays are widely used as tower internals and their choice is due to economical attractiveness. While operating a trayed distillation tower weeping phenomenon has a critical effect on the efficiency, in this case study a weeping phenomenon was undertaken by means of numerical model in a rectangular sieve tray. Eulerian-Eulerian Computational Fluid Dynamics (CFD) method was used and the obtained CFD results are in a good agreement with the experimental data in terms of weeping rate and pressure drop.

Key Words : CFD, Multiphase Flow, Hydrodynamics, Rectangular Sieve Tray, Weeping

1. Introduction

In distillation which is by far the most widely used method for separating liquid mixtures, low cost and simplicity in construction have made sieve trays the most widely used distillation column internals. Despite the thereof attractiveness efficiency associated with sieve tray is low. Furthermore, due to low thermodynamic efficiency, distillation process requires considerable amounts of external energy to perform the separation [1].

As for operability of distillation column, there

[†] Dept.of Naval Architecture and
  Ocean Engineering, Pusan National University
  E-mail: inwon@pusan.ac.kr
[*] Global Core Research Center for Ships and
  Offshore Plants, Pusan National University

exists a range of operating conditions (operating window, Fig. 1 in which trays have a good operating flexibility. The window of satisfactory operation is bounded by undesirable conditions such as flooding, entrainment and weeping. At low values of flow parameter (FLG), weeping occurs whereby liquid passes through the plate perforations. The flow parameter represents a ratio of liquid to vapor kinetic energies. In ideal case, the liquid carries no vapor bubbles to the tray below and the vapor carries no liquid droplets to the tray above (entrainment) which is due to high vapor velocity, and there is no weeping of liquid through the openings of the tray (plate perforations) [1].

Furthermore, to use tray towers more effectively, a theoretical understanding of tray hydraulics is essential. As alternative way to surpass the use of many experiments that may be required to describe

the flow pattern inside complex geometries such as sieve tray into distillation column, computer simulation techniques are nowadays utilized to predict tray hydraulics and get better understanding of tray behavior. In this context, computational fluid dynamics (CFD) has become a potent tool in complement to experimental work to investigate the hydraulic parameters of tray towers and prediction of the tray efficiency. Several study cases that consider CFD modeling of the trays of distillation column have been published [2-7].

Different researchers have worked on flow hydraulics on trays, some of them have noticed symmetric flow fields about the tray center [8, 9]; and thereafter different researchers have modeled half of the tray geometry to study hydraulic parameters on column tray [10-12]. For sieve tray operated at weeping conditions, Mehta [10] studied the hydraulic of half of circular sieve tray using CFD while Zarei et al. [13] studied the hydraulic of half of a rectangular sieve tray column to investigate the liquid weeping. They observed that the weeping phenomenon does not distribute uniformly over the tray.

Throughout this paper, a CFD model is developed to describe tray hydraulic behavior for the operating conditions in which weeping occurs. The results are then compared with experimental data [14] as a validation step.
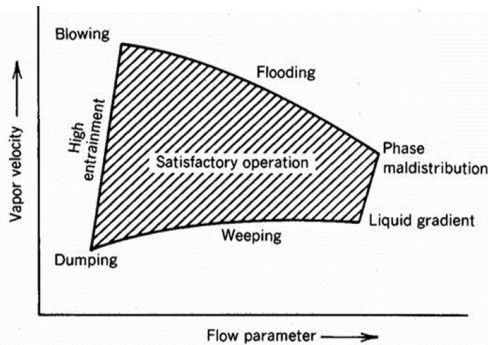

Fig. 1. Performance diagram for tray columns.

2. CFD model development

2.1 Model governing equations

The model governing equations include the flow of gas and liquid in the Eulerian framework whereby each phase is treated as interpenetrating continuum with separate transport equations. The continuity and momentum equations were numerically solved for each phase.

Continuity equations for gas and liquid phases:

$$\frac{\partial(\alpha_G \rho_G)}{\partial t} + \nabla . (\alpha_G \rho_G u_G) = S_{GL} \tag{1}$$

$$\frac{\partial(\alpha_L \rho_L)}{\partial t} + \nabla . (\alpha_L \rho_L u_L) = -S_{GL} \tag{2}$$

Where u is velocity vector, subscript G and L correspond to gas and liquid phase respectively, ρ is density, SLG is the rate of mass transfer from liquid phase to gas phase and vice versa. Mass transfer between the two phases must satisfy the local balance condition (SGL = -SLG), for the present case study mass transfer is not expected, hence SGL -SLG =0.

Momentum equations for gas and liquid phases:

$$\frac{\partial(\alpha_G \rho_G u_G)}{\partial t} + \nabla . \left(\alpha_G (\rho_G u_G u_G)\right) =$$
$$\nabla . \left(\alpha_G \mu_{eff,G} (\nabla u_G + (\nabla u_G)^T)\right) - \alpha_G \nabla p_G -$$
$$M_{GL} + \alpha_G \rho_G g \tag{3}$$

$$\frac{\partial(\alpha_L \rho_L u_L)}{\partial t} + \nabla . \left(\alpha_L (\rho_L u_L u_L)\right) =$$
$$\nabla . \left(\alpha_L \mu_{eff,L} (\nabla u_L + (\nabla u_L)^T)\right) - \alpha_L \nabla p_L +$$
$$M_{GL} + \alpha_L \rho_L g \tag{4}$$

where μeff is effective viscosity, g is gravity acceleration. For solving model governing equations for velocities, pressure, and volume fractions, closure relationship equations are necessary to relate the interphase momentum transfer term M and the turbulent viscosities to the mean flow variables. Volume fractions of gas and liquid are constrained through the following relation

$$\alpha_L + \alpha_G = 1 \tag{5}$$

The same pressure field is assumed for both phases, thus

$$p_L = p_G \tag{6}$$

As for interphase momentum transfer term,

$$M_{GL} = \frac{3C_D}{4d_G}\alpha_L\rho_L|u_G - u_L|(u_G - u_L) \tag{7}$$

where $\quad C_D = \frac{24}{R_e}, \quad R_e \ll 1 \quad$ or

$$C_D = 0.44, \quad 1000 \le R_e \le 1\sim2*10^5$$

d_G is mean bubble diameter. Add that interphase momentum transfer term describes the interfacial forces (drag force, virtual mass force, and lift force) acting on each phase due to the presence of the other phase. Among the interfacial forces, virtual mass force, and lift force do not affect the bubble flow greatly like drag force does and can be ignored in this work.

For the rise of a swarm of large bubbles in the Churn-turbulent regime, drag coefficient is evaluated as follows:

$$C_D = \frac{4}{3}\frac{\rho_L - \rho_G}{\rho_L}gd_G\frac{1}{V_{slip}^2} \tag{8}$$

$$V_{slip} = \frac{U_G}{\gamma_G} \tag{9}$$

Table 1. Specifications of rectangular sieve tray.

Plate active area	0.6118 m^2
Hole area %	6.83
Number of holes	328
Number of trays	2
Hole diameter	12.7 mm
Tray thickness	3 mm
Weir height	50 mm
Downcomer clearance	50 mm
Weir length	630 mm
Tray length	1.20 m

V_{slip} is the slip velocity of the bubble swarm with respect to liquid. Average vapor holdup fraction ($\overline{\gamma_G}$) is expressed as follows [3]:

$$\overline{\gamma_G} = 1 - \exp\left[-12.55\left(U_s\sqrt{\frac{\rho_G}{\rho_L - \rho_G}}\right)^{0.91}\right] \tag{10}$$

where Us corresponds to gas superficial velocity.

2.2 Free Surface Model "VOF-like method"

In this study, ANSYS CFX 18.2 software was used to carry out the simulations. Free Surface Model which is "VOF-like method" is provided for multiphase calculations and it is used to allow the two phases to separate when incorporated with inhomogeneous model. It is introduced for the calculation of the interface between the fluids. Surface tension model
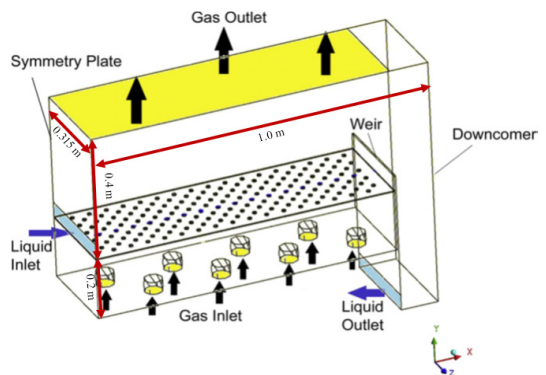

Fig. 2. Geometry of simulated tray [13].

used in CFX is based on the continuum surface force (CSF) model of Brackbill and models the surface tension force as a volume force concentrated at the interface rather than a surface force [15].

2.3 Geometry and boundary conditions

The specifications of computational domain are summarized into Table 1 and schematically illustrated into Figure 2. Geometry and operating conditions of the model are exactly based on geometry used in experimental tests as reported into [14]. The actual dimensions of the tray were simulated, the inlets for gas which is air in this case are chimneys mounted on chamber floor below the test tray. The chimneys are of 7.5 cm height and the chamber is 20 cm height below the tray deck, by assumption this chamber leads to better and more realistic gas distribution to the tray.

The mass-flow inlets were specified for both liquid and gas phases. For liquid inlet, only liquid which is water was assumed to enter the flow geometry and only gas (air) was assumed to get into gas inlet. Constant mass fraction values for entering gas and liquid phases were used. At the outlets, air outlet was specified as an opening boundary through which only air is allowed to escape from with static pressure of atmospheric pressure; as for the liquid outlet boundary it was specified as wall. For wall boundaries, a no-slip wall boundary condition was specified for the liquid phase and a free slip wall boundary condition for the gas phase. All of the walls were assumed as smooth wall boundary, and a volume fraction contact model was used. In regard to volume fraction contact model; for the momentum equation, the volume fraction of a given phase is multiplied by the total wall shear stress to determine the component of wall shear stress that is due to that phase.

2.4 Geometry meshing

Referring to the complexity of the simulated geometry, the nonconformal meshing strategy is applied to reduce the number of cells. The perforations on the tray are extruded and added to the chamber below the tray to form one body which was meshed with hexahedral dominant method. The chamber above the tray which has a simple geometrical shape was meshed through sweep method with hexahedral cells. The denser grids were then produced near the tray floor in order to achieve greater numerical accuracy and better flow visualization in that region; away from the tray deck, the mesh sizes became larger. Grid independence of the solution was achieved by a total number of computational cells of 625,986, which was found to be sufficiently accurate.

3. Results and discussions

3.1 Liquid phase weeping

A liquid loading of Q_L = 0.00525 m^3/s and various values of gas loading factor, F_s, (0.38, 0.55 and 1.034 m/s(kg/m^3)$^{0.5}$) are used. During simulation runs, investigated hydraulic parameters were calculated by the CFD model after reaching the quasi-steady state to avoid start up effects on the results. The height of liquid that would exist on the tray in the absence of vapor flow is regarded as clear-liquid height; hence, the clear liquid height was calculated as the tray spacing multiplied by the average volume fraction of the liquid phase above the bubbling area of the tray floor.

Fig. 3 shows a comparison between the experimental data and CFD results in terms of weeping rate for QL = 0.00525 m^3/s for three values of air loading factors, Fs. From both results, a common trend shows that the weeping rates decrease as gas flow factor (Fs) increases. This is obvious because decreasing gas flow factor results in reducing gas drag force that is being exerted on the liquid phase, which leads to increasing the wept liquid throughout the tray perforations.
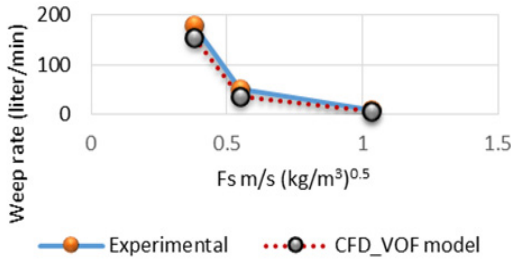
Fig. 3. Weeping rate for QL = 0.00525 m3/s.

3.2 Dry tray pressure drop

Among important hydraulic parameters, dry tray pressure drop is one of them and affects liquid weeping occurrence. For the present study case, the trend of CFD results for dry pressure drop is compared with correlation of Zuiderweg. Fig. 4 illustrates a comparison between the dry tray pressure drops predicted by CFD and the thereof correlation.
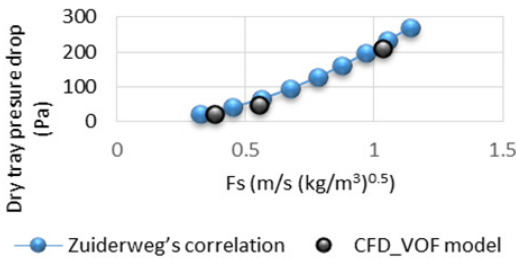

Fig. 4. Comparison between the dry tray pressure drops predicted by CFD tool and the correlation of Zuiderweg.

For further visualization, Fig. 5 shows the instantaneous predicted liquid volume fraction on ZY cross section and X = 0.145 m for two values of Fs, i.e. 0.38 and 0.55 m/s(kg/m^3)$^{0.5}$ respectively, after 6 seconds of computational time. Fig. 6 shows the contour plot of liquid volume fraction at 3.5 cm above the tray deck for 0.38 and 0.55 m/s(kg/m^3)$^{0.5}$ air loading factors after 6 seconds of computational time. As it can be seen from the two respective figures, the levels of wept liquid are distinctive (the wept liquid is observed clearly on the chimney tray, Fig. 5); this confirms the trend that was noticed
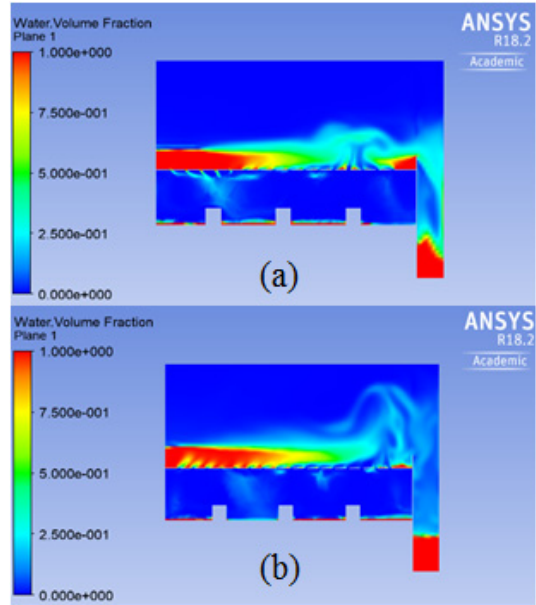

Fig. 5. Contours plot of liquid volume fraction snapshot at QL = 0.00525 m3/s for (a) FS = 0.38 m/s (kg/m^3)$^{0.5}$ and (b) Fs = 0.55 m/s (kg/m3)$^{0.5}$.
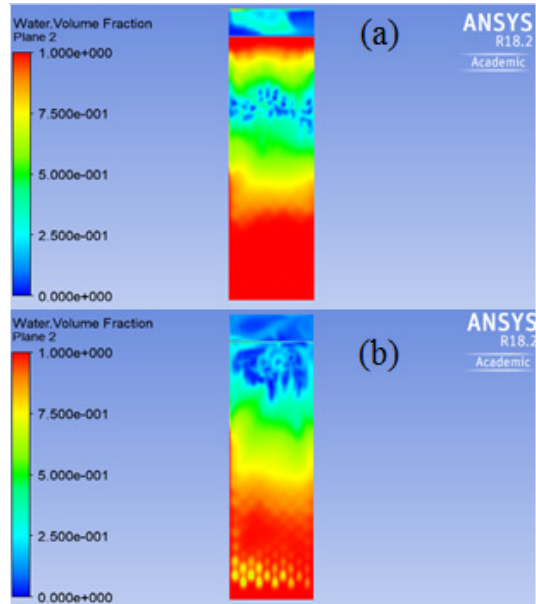

Fig. 6. Contours plot of liquid volume fraction snapshot at 3.5 cm above the tray deck at QL = 0.00525 m^3/s for (a) FS = 0.38 m/s (kg/m^3)$^{0.5}$ and (b) Fs = 0.55 m/s (kg/m^3)$^{0.5}$.

throughout Fig. 3, where the weeping rates decrease as gas flow factor increases.

The distribution of liquid over the tray is not uniform, while the liquid (water) enters through liquid inlet gas phase (air) seeks to find an escape and crosses through liquid at the other side (weir side). During the passage of air the liquid is pushed and accumulates at one side, Figure 5a; a thick layer of liquid is accumulated near liquid inlet and results into weeping. As the liquid continues to accumulate, at a certain point it flows over while gas pushes the liquid (gas drag force that is exerted on the liquid phase) and finds another escape while crossing through liquid at the place that was weeping previously, Figure 5b.

4. Conclusion

The comparison between CFD results and experimental data shows a good compatibility in terms of weeping rate. Furthermore, our results are in a good agreement with some empirical correlations in terms of dry pressure. In addition, the model predicted some hydraulic parameters such as liquid volume fraction on the tray and downcomer. Based on simulation results, CFD is an impeccable and effective tool that can be used to investigate and provide detailed information on gas and liquid flows into distillation column containing rectangular sieve trays.

ACKNOWLEDGEMENT

REFERENCE

1) Seader, J. D. and Henley, E. J., 1998, "Separation Process Principles," John Wiley & Sons, Inc., New York, pp. 508-509.

2) Krishna, R., Van Baten, J. M., Ellenberger, J., Higler, A. P., Taylor, R., 1999, "CFD simulations of sieve tray hydrodynamics," Chem. Eng. Res. Des. 77, pp. 639-646.

3) Van Baten, J. M. and Krishna, R., 2000, "Modelling sieve trays hydraulics using computational fluid dynamics," Chem. Eng. J. 77, pp. 143-151.

4) Trujillo, F. J., Lovatt, S. J., Harris, M. B., Willix, J., Pham, Q. T., 2003, "CFD modeling of the heat and mass transfer process during the evaporation of water from a circular cylinder," The Proceedings of the 3rd International Conference on CFD in the Minerals and Process Industries, CSIRO, Melbourne, Australia, pp. 99-104.

5) Li, X. G., Liu, D. X., Xu, S. M., Li, H., 2009, "CFD simulation of hydrodynamics of valve tray," Chem. Eng. Process, 48, pp. 145-151.

6) Zarei, T., Rahimi, R., Zivdar M, 2009, "Computational fluid dynamic simulation of MVG tray hydraulics," Korean J. Chem. Eng., 26, pp. 1213-1219.

7) Alizadehdakhel, A., Rahimi, M., Alisairafi, A. A., 2010, "CFD and experimental studies on the effect of valve weight on performance of a valve tray column," Comput. Chem. Eng., 34, pp. 1-8.

8) Solari, R. B., Saez, E., D'apollo, I., Bellet, A., 1982, "Velocity distribution and liquid flow patterns on industrial sieve trays," Chem. Eng. Commun. 13, 369-384.

9) Solari, R. B., Bell, R. L., 1986, "Fluid flow patterns and velocity distribution on commercial-scale sieve trays," AIChE J., 32, pp. 640-649.

10) Mehta, B., Chuang, K. T., Nandakumar, K., 1998, "Model for liquid phase flow on sieve trays," Chem. Eng. Res. Des., 76, pp. 843-848.

11) Liu, C. J., Yuan, X. G., Yu, K. T., Zhu, X. J., 2000, "A fluid dynamic model for flow pattern on a distillation tray," Chem. Eng. Sci., 55, pp. 2287-2294.

12) Rahimi, R., Rahimi, M. R., Shahraki, F., Zivdar, M.,

2006, "Efficiencies of sieve tray distillation columns by CFD simulations," Chem. Eng. Technol., pp. 326-335.

13) Zarei, A., Hosseini, S. H., Rahimi, R., 2013, "CFD study of weeping rate in the rectangular sieve trays," J. Taiwan Inst. Chem. Eng., 44, pp. 27-33.

14) Lockett M. J. and Banik S., 1986, "Weeping from sieve trays," Ind. Eng. Process Des. Dev., 25, pp. 561-569.

15) ANSYS, Inc., 2013, "Ansys CFX solver theory guide", Southpointe 275 Technology drive Canonsburg, PA 15317, Release 15.